X-Ray tomography-based microstructure representation in the Snow Microwave Radiative Transfer model

Sandells, M., Lowe, H., Picard, G., Dumont, M., Essery, R., Floury, N., Kontu, A., Lemmetyinen, J., Maslanka, W. ORCID: https://orcid.org/0000-0002-1777-733X, Morin, S., Wiesmann, A. and Matzler, C. (2022) X-Ray tomography-based microstructure representation in the Snow Microwave Radiative Transfer model. IEEE Transactions on Geoscience and Remote Sensing, 60. ISSN 0196-2892 doi: https://doi.org/10.1109/TGRS.2021.3086412 Available at https://centaur.reading.ac.uk/101250/

X-Ray Tomography-Based Microstructure Representation in the Snow Microwave Radiative Transfer Model

Melody Sandells, Henning Löwe, Ghislain Picard, Marie Dumont, Richard Essery, Nicolas Floury, Anna Kontu, Juha Lemmetyinen, William Maslanka, Samuel Morin, Andreas Wiesmann, *Senior Member, IEEE*, and Christian Mätzler

***Abstract*— The modular Snow Microwave Radiative Transfer (SMRT) model simulates microwave scattering behavior in snow via different selectable theories and snow microstructure representations, which is well suited to intercomparisons analyses. Here, five microstructure models were parameterized from X-ray tomography and thin-section images of snow samples and evaluated with SMRT. Three field experiments provided observations of scattering and absorption coefficients, brightness temperature, and/or backscatter with the increasing complexity of snowpack. These took place in Sodankylä, Finland, and Weissfluhjoch, Switzerland. Simulations of scattering and absorption coefficients agreed well with observations, with higher errors for snow with predominantly vertical structures. For simulation of brightness temperature, difficulty in retrieving stickiness with the Sticky Hard Sphere microstructure model resulted in relatively poor performance for two experiments, but good agreement for the third. Exponential microstructure gave generally good results, near to the best performing models for two field experiments. The Independent Sphere model gave intermediate results. New Teubner–Strey and Gaussian Random Field models demonstrated the advantages of SMRT over microwave models with restricted microstructural geometry. Relative model performance is assessed by the quality of the microstructure model fit to micro-computed tomography (CT) data and further improvements may be possible with different fitting techniques. Careful consideration of simulation stratigraphy is required in this new era of high-resolution microstructure measurement as layers thinner than the wavelength introduce artificial scattering boundaries not seen by the instrument.**

Manuscript received September 25, 2020; revised February 17, 2021 and April 27, 2021; accepted May 17, 2021. This work was supported in part by the European Space Agency under Grant ESTEC:4000112698/14/NL/LvH. *(Corresponding author: Melody Sandells.)*

Melody Sandells is with the Department of Geography and Environmental Sciences, Northumbria University, Newcastle upon Tyne NE1 8ST, U.K. (e-mail: melody.sandells@northumbria.ac.uk).

Henning Löwe is with the WSL Institute for Snow and Avalanche Research SLF, 7260 Davos, Switzerland.

Ghislain Picard is with IGE, Université Grenoble Alpes, 38402 Grenoble, France.

Marie Dumont and Samuel Morin are with Météo-France, Center d'Études de la Neige, CNRS, CNRM, Université Grenoble Alpes, 38400 Grenoble, France.

Richard Essery is with the School of GeoSciences, The University of Edinburgh, Edinburgh EH9 3FF, U.K.

Nicolas Floury is with ESA-ESTEC, 2200 AZ Noordwijk, The Netherlands.

Anna Kontu and Juha Lemmetyinen are with the Finnish Meteorological Institute, FI-00560 Helsinki, Finland.

William Maslanka is with the Department of Geography and Environmental Science, University of Reading, Reading RG6 6AB, U.K.

Andreas Wiesmann and Christian Mätzler are with Gamma Remote Sensing AG, 3073 Gümligen, Switzerland.

Digital Object Identifier 10.1109/TGRS.2021.3086412

***Index Terms*— Microstructure, microwave scattering, SMRT model, snow, snow microwave radiative transfer (SMRT).**

I. Introduction

SNOW microstructure knowledge is essential to determine the scattering properties of snow at microwave frequencies. Simulations of microwave scattering are used as the basis for remote sensing of snow mass for water resources and may be used to investigate how the snow mass has changed over the last few decades. The Snow Microwave Radiative Transfer (SMRT) model has recently been developed in order to examine the impact of the representation of the microstructure, to provide consistent theoretical treatment for passive and active simulations, and as a basis for a community model open to future developments [1]. This article provides a thorough evaluation of the SMRT model against observations from three different field campaigns.

Many previous simulations of microwave emission and scattering in the snow using inputs from *in situ* measurements or snowpack evolution model simulations have a common feature: scaling of the microstructure parameters is applied in order to obtain reasonable comparison with observed radiometric data. Scaling has been applied to observations of traditional grain size [2] as used in the Helsinki University of Technology (HUT) model [3], [4], exponential correlation length [5] as used in the Microwave Emission Model of Layered Snowpacks (MEMLS) [6], [7], and sticky hard sphere (SHS) [8] as used by models based on Dense Media Radiative Transfer (DMRT) theory [9]. Stickiness is a secondary (dimensionless) parameter used in the SHS microstructure model and represents the degree of clustering between individual grains. A number of intercomparison studies between these models has illustrated different scaling factors required for each model [10]–[13]. Stickiness itself is a challenging parameter to quantify [14].

Traditional grain size is a notoriously observer-dependent measurement and is largely incompatible with the accuracy requirements for the snow microstructure of around 0.01–0.04 mm [15]. In recent years, new instruments have been developed to measure the snow microstructure in the field from reflectivity measurements at near-infrared wavelengths [16], which gives snow specific surface area (SSA) from which an optical grain diameter can be determined.

Other methods of determining SSA include gas adsorption, and microcomputed X-ray tomography [17] [micro-computed tomography (CT)]. However, SSA only is insufficient to fully parameterize microstructure models. Micro-CT can provide the missing information because it gives a 3-D reconstruction of the ice-air matrix from which the correlation function may be calculated and the parameters of the analytical correlation functions can be fit to the observed correlation function.

Until recently, microwave scattering models have not kept up to date with the developments in snow microstructure observation techniques. SMRT was developed in part as a response to new instruments, especially micro-CT, but also from a demonstration of the sensitivity to microstructure [15] and a need for more than one microstructure length scale. SMRT was evaluated against a substantial dataset of Arctic and sub-Arctic snow in [18] for SHS and exponential microstructure. The present article is the first to use tomographic microstructure observations to provide an extensive evaluation of the performance of SMRT against field observations for all SMRT microstructure models.

The evaluation is conducted in three steps, with data from three different field campaigns. The first step is a fundamental evaluation of the scattering and absorption coefficients given detailed microstructure information from micro-CT samples acquired during the Arctic Snow Microstructure Experiment (ASMEx) [19]. The second step is an evaluation of a shallow snowpack simulation of brightness temperature with a very simple lower boundary condition, with snowpack correlation functions given by analysis of thin section images acquired with the Passive and Active Microwave and Infrared Radiometer (PAMIR) instrument [20]. The third step is the evaluation of the active portion of the model given a snapshot of the micro-CT profile of a complete snowpack with natural substrate and to present simulations of the angular dependence of both brightness temperature and backscatter. Data are from the Nordic Snow Radar Experiment (NoSREx) [21].

Section II presents a brief description of SMRT. The three field campaigns and the simulation methodology are described in Section III. Results are given in Section IV followed by discussions and conclusions in Sections V and VI.

II. SMRT Model

The SMRT model [1] was developed in response to increased understanding of the importance of microstructure parameterization in snow, and to enable isolation of individual model components in microwave scattering model intercomparison studies. For this, SMRT has a modular structure, which clearly separates the different steps of the calculation (permittivities of the raw materials, scattering coefficients, and solution of the radiative transfer (RT) equation), and for each step offers different theoretical assumptions or theories that can be selected by the user. To facilitate the modular nature, SMRT is written in Python with object-oriented programming techniques and a plugin system. It has been released to the community under an open-source license (see Section VII on code availability) in order to allow it to be used as a general framework for future developments.

For an evaluation of SMRT in this article, correlation functions of the snow were determined from field samples. To focus on the microstructure model approaches, the Improved Born Approximation (IBA) was used as the electromagnetic model for all the simulations in this article. Other theories available in SMRT to compute scattering are specific to a particular microstructure form (e.g., DMRT quasi-crystalline approximation (QCA) is for SHS only). In IBA, the bistatic scattering coefficient (also known as the phase function) is defined for a 2-phase medium (subscript 1 denotes the host constituent and subscript 2 denotes the scattering constituent). Radiation from the direction given by zenith and azimuth angles ϑ', φ' is scattered into ϑ, φ, according to [22]

$$p\ (\vartheta, \varphi, \vartheta', \varphi') = f_2(1-f_2)(\epsilon_2-\epsilon_1)^2\ Y^2(\epsilon_1,\epsilon_2)\ M(|\mathbf{k}_d|)\ k_0^4 \sin^2\chi \quad (1)$$

where f_2 is the fractional volume of the scattering constituent, ϵ is the permittivity, Y^2 is the mean squared field ratio i.e., ratio of the field inside the scattering materials to that incident on it, $M(|\mathbf{k}_d|)$ is the microstructure function, k_0 is the wavevector in free space and χ is the polarization angle. The microstructure function in IBA is determined from the Fourier transform (FT) of the correlation function $\widetilde{C}(|\mathbf{k}_d|)$, as described by [1], [14]. $\mathbf{k}_d$ is the wavevector difference between scattering and incidence angles and is dependent on the effective permittivity of the medium computed with the Polder–Van Santen mixing formula [23]. For this implementation of SMRT, the simplification of spherical symmetry has been applied for scattering, which means that $|\mathbf{k}_d|$ can be replaced with k_d. The microstructure function can then be calculated as

$$M(k_d) = \frac{1}{4\pi}\frac{\widetilde{C}(k_d)}{f_2(1-f_2)}. \quad (2)$$

As with any model, IBA is a theory with limitations. At present, only two constituents may be represented (here, ice and air). To allow an arbitrary arrangement of scattering material within the medium, the propagation speed is assumed constant throughout the snow layer. In this implementation, the relationship between the electric field inside scatterers and that outside is assumed to be the same as for spherical scatterers as this ratio is more dependent on the volume fraction than the type of scatterer [22]. Despite limitations specific to IBA, IBA remains closely related to DMRT theory, at least in the low-frequency limit [14]. DMRT was shown to be limited to small and moderate densities [24], [25], which is likely to apply to IBA, but needs further comparison with exact electromagnetic calculations. SMRT allows a comparison between IBA and DMRT at higher frequencies but is not considered in this article due to the SHS microstructure restriction in DMRT.

For the simulations in this article, five different microstructure models were used: spherical model also known as independent sphere (IND), SHS, exponential (EXP), Teubner–Strey (TS), and Gaussian Random Field (GRF). Analytical expressions for the correlation functions in Fourier space as required by (2) exist for all but the GRF model. $\widetilde{C}(k_d)$ for the SHS model, which requires sphere radius and stickiness as

parameters, was given in 31 of [14]. The microstructure functions in Fourier space for the IND, EXP, and TS models are

$$\widetilde{C}_{\mathrm{IND}}(k) = f_2(1-f_2)\left(\frac{\pi d_{\mathrm{ind}}^3}{6}\right)\left[\frac{3(\sin X - X\cos X)}{X^3}\right]^2 \quad (3)$$

$$X = k_d d_{\mathrm{ind}}/2$$

$$\widetilde{C}_{\mathrm{EXP}}(k_d) = \frac{8\pi l_{\mathrm{ex}}^3 f_2(1-f_2)}{[1+(k_d l_{\mathrm{ex}})^2]^2} \quad (4)$$

$$\widetilde{C}_{\mathrm{TS}}(k_d) = \frac{8\pi \xi_{\mathrm{TS}}^3 f_2(1-f_2)}{[1+Z]^2 + 2[1-Z](k_d\xi_{\mathrm{TS}})^2 + (k_d\xi_{\mathrm{TS}})^4}$$

$$Z = \left(\frac{2\pi\xi_{\mathrm{TS}}}{d_{\mathrm{TS}}}\right)^2 \quad (5)$$

where d_{ind} is the IND diameter, l_{ex} is the exponential correlation length, ξ_{TS} is the TS correlation length and d_{TS} is the TS domain length (also known as repeat distance).

For GRF, numerical calculation of the FT of the correlation function has been applied as an analytical form cannot be found. The GRF real space correlation function (as a function of distance r) is given as

$$C_{\mathrm{GRF}}(r) = f_2(1-f_2)\frac{1}{2\pi}\int_0^{C_\psi(r)} \frac{1}{\sqrt{1-t^2}}\exp\left[-\frac{\beta^2}{1+t}\right]dt \quad (6)$$

where β is a cut-level parameter ([26]) related to the volume fraction. The correlation function of the underlying random field currently used for the GRF in SMRT is

$$C_\psi(r) = \exp(-r/\xi_{\mathrm{grf}})\left(1+\frac{r}{\xi_{\mathrm{grf}}}\right)\frac{\sin(2\pi r/d_{\mathrm{grf}})}{(2\pi r/d_{\mathrm{grf}})} \quad (7)$$

where ξ_{grf} is the GRF correlation length and d_{grf} is the GRF domain length (or repeat distance).

The RT solver in SMRT is based on the Discrete Ordinates (DORT) approach with stream matching at the boundaries as described in [1]. Fourier decomposition is used to deal with the azimuthal dependence of the phase function and allows computation of the general solution of the RT equations by eigenanalysis, while the particular solution is obtained by solving a linear system representing the boundary conditions. So, it is the FT of the IBA phase function with respect to the azimuthal component that is used by the solver. The evaluation is done numerically.

Section III describes the three field campaigns with sufficient microstructural data to evaluate SMRT for all implemented microstructure models. Each dataset and simulation methodology are described in turn.

III. Evaluation Data Description and Methods

Fitting of the microstructure models to the micro-CT data followed a common procedure for all datasets. This is described in Section III-D, after the descriptions of individual field experiments.

A. Arctic Snow Microstructure Experiment (ASMEx)

The ASMEx [19] took place in Sodankylä, Finland in the winters of 2013–2014 and 2014–2015. This field campaign was specifically designed to measure scattering and absorption coefficients of slabs of homogeneous snow in order to develop a new snow extinction coefficient model as a function of SSA for the HUT snow emission model [4], [27]. Data from this campaign included micro-CT samples and therefore provide an ideal dataset to evaluate the SMRT microstructure and electromagnetic components of the model independently of the solver. This section provides a brief description of the field measurement methodology, retrieval of scattering and absorption coefficients, and simulation approach. A total of 14 horizontal snow slabs (width = 60 cm, length = 80 cm, various heights) were extracted and observed with microwave radiometers during the ASMEx field campaign.

Brightness temperatures (T_B)s of the snow slabs were measured on 1) a metal (highly reflecting) base and 2) microwave absorber (highly absorbing) base [27] at frequencies of 18.7, 21, 36.5, 90, and 150 GHz. A metal sheet was used to transfer the snow slab from the natural snowpack onto microwave absorbers where the metal base observations were made. The metal sheet was then carefully slid from under the snow slab to allow the snow slab to rest on the microwave absorber, as described in [19]. Measurement error specification for these instruments is 1 K, independently confirmed for 18.7–90 GHz by [21]. For ASMEx, the measurement protocol was similar in each case, with minor differences in absorber material used and frequency range observed due to equipment availability, as described in [28]. Destructive sampling of the snow slabs was then carried out roughly in order from least destructive to most destructive as described by [28]. Snow micropenetrometer profile measurements were taken first, followed by temperature, density then SSA profiles within the slab. Snow grain macro photographs were also taken after SSA observations. Finally, two samples of cross section 5 cm × 5 cm (height of slab governs the third dimension, typically around 15 cm) were taken [28], one from the radiometer center of field of view and another in close proximity. These samples were cast in di-ethyl pththalate in the field, transported to the WSL Institute for Snow and Avalanche Research SLF in Davos, Switzerland, where they were processed and observed with an X-ray microtomography (micro-CT) instrument.

A total of 14 slabs were observed over the two winter seasons: slabs A01-A07 in the first season and slabs B01-B07 in the second. The orientation of micro-CT samples from slab A01 differed from the remaining slabs as horizontal rather than vertical profiles were taken, and only one cast sample was taken for slab A02 (for calculation of error statistics, the second A02 sample was assumed to be the same as the first). Cylindrical sections were extracted from the vertically casted snow samples and cut in half in order to fit into the micro-CT instrument, as illustrated by Fig. 1. This means that a small section of snow is missing due to the thickness of the saw, although this gap is neglected for analysis purposes. Snow parameters were then determined for smaller overlapping cubic subsamples within each micro-CT sample.

Snow density and SSA were calculated from 120 voxel height subsamples, which corresponds to a subsample height of 2.18 mm. Mean density and SSA for each of the slab is shown in Fig. 2. Although the slabs were visually

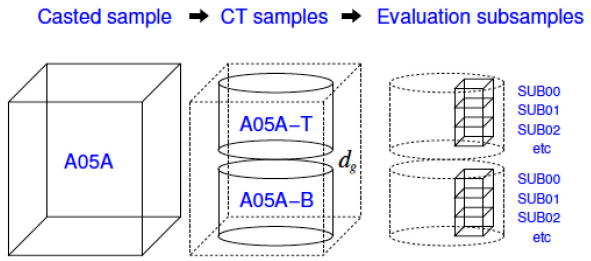

Fig. 1. Processing of slab samples (except slab A01): Slab samples were sliced into two micro-CT samples, and scanned with a nominal resolution (voxel size) of 18 μm. Microstructure parameters were calculated over 10.8 mm stacked, overlapping subsamples.

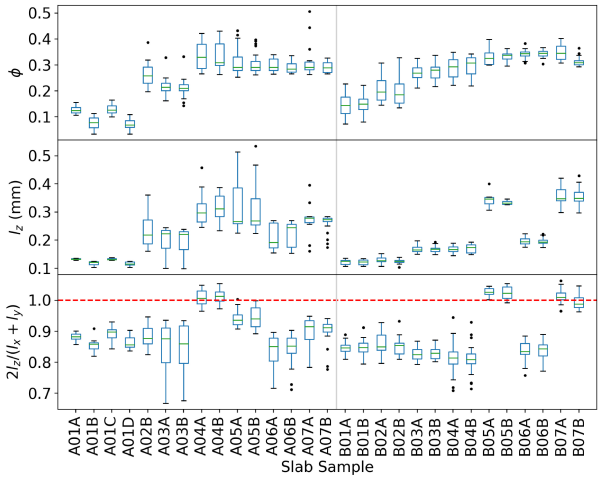

Fig. 2. Microstructure properties for 14 ASMEx slab subsamples. Gray line separates samples taken in two different seasons. (Top) Fractional volume of ice. (Middle) Correlation length in vertical direction. (Bottom) Ratio of vertical correlation length to horizontal correlation length (anisotropy).

homogeneous at the point of extraction, the density and SSA range within each slab show that they are not strictly homogeneous. Early in the season (lower slab samples) the slabs are characterized by lower density and smaller microstructure scales/sizes; both generally increase as the season progresses. Perfectly isotropic snow would have equal horizontal and vertical correlation lengths i.e., anisotropy factor 2 $\ell_z/(\ell_x + \ell_y) = 1$ as shown by the red dashed line in Fig. 2. An anisotropy factor of less than 1 means the correlation length is larger in the horizontal direction than the vertical, which is the case for the majority of slab samples, as expected for surface snow that has hardly undergone any temperature gradient metamorphism [29]. The microstructure is larger in the vertical for slabs A04, B05, and B07 only. Spherical symmetry is assumed in the version of SMRT used in this article, which may not be appropriate and is discussed later in this article.

Correlation functions of the snow were determined from the 3-D structure of the ice matrix and parameters retrieved for the five analytical correlation function models by minimization of the cost function (further details given below). A summary of microstructure parameters for all slabs is given in Table I.

Density and microstructure parameters were used to calculate scattering and absorption coefficients for each micro-

TABLE I

SUMMARY OF MICROSTRUCTURAL PROPERTIES FOR ALL THREE EXPERIMENTS (IQR IS INTERQUARTILE RANGE). ASMEX AND NOSREX PARAMETERS WERE DERIVED FROM MICRO-CT DATA, PAMIR PARAMETERS WERE DERIVED FROM THIN SECTION IMAGES. DENSITY IS GIVEN IN Kg m^{-3}, τ IS DIMENSIONLESS, ALL OTHER MICROSTRUCTURAL PARAMETERS ARE GIVEN IN mm. ASMEX, PAMIR AND NOSREX DATASETS HAVE 562, 10 AND 320 SUBAMPLES, RESPECTIVELY

	ASMEx		PAMIR		NoSREx	
	Median	IQR	Median	IQR	Median	IQR
Density	258	95	397	66	217	87
d_{SHS}	0.50	0.38	0.80	0.38	0.15	0.16
τ	0.10	0.12	0.10	0.05	0.11	0.02
l_{ex}	0.14	0.09	0.46	0.12	0.11	0.15
d_{IND}	0.41	0.28	1.23	0.31	0.32	0.44
ξ_{TS}	0.20	0.13	0.53	0.15	0.14	0.19
d_{TS}	1.46	2.67	502	340	2.21	333
ξ_{GRD}	0.14	0.10	0.37	0.11	0.10	0.14
d_{GRF}	1.70	33)	485	333	8.12	334

CT subsample to evaluate SMRT scattering theories independently of other SMRT modules (namely the RT solver, substrate, atmosphere, and interface modules). Simulations of the absorption and scattering coefficients were carried out for all slab subsamples at all ASMEx frequencies for all five microstructure models. Slab means of these subsample coefficients were compared against the bulk slab coefficients retrieved from the radiometric data by [27]. As described in [27], there is a difference between coefficients retrieved from horizontally and vertically polarized observations. Here, the mean of the coefficients derived at both polarizations is used as the observations for comparison with SMRT.

For calculation of T_B, the slabs were reconstructed from the micro-CT subsamples with one snowpack layer corresponding to one micro-CT subsample with layer thickness scaled to account for mass lost during micro-CT preparation. For the simulations, the substrate was assumed to be a perfect reflector for the metal plate case, whereas for the absorber substrate, the reflectivity was determined from the measured emissivity. Where absorber emissivity observations were not available, the mean of all observations at that frequency was used. Measured downwelling atmospheric T_B was used to parameterize the simple isotropic atmosphere in SMRT (a single plane parallel layer that follows MEMLS formulation [30]) and included in simulation of T_B.

B. Passive and Active Microwave and Infrared Radiometer (PAMIR) Snow Crust Experiment

The PAMIR system included five microwave radiometers at frequencies 4.9, 10.4, 21, 35, and 94 GHz (measurement error ~1 K at 260 K [31]) mounted on a 15 m tower at an incidence angle of 50° at the Weissfluhjoch, Davos site from 1977 to 1987. Here, we describe a snow crust experiment that took place 8–10 May 1984 when the snowpack underwent two melt-refreeze cycles. The depth of refrozen snow was measured manually and the snowpack observed with PAMIR over the course of the experiment (33 measurements over 41 h) [20] and two thin section images were taken, shown in Fig. 3.

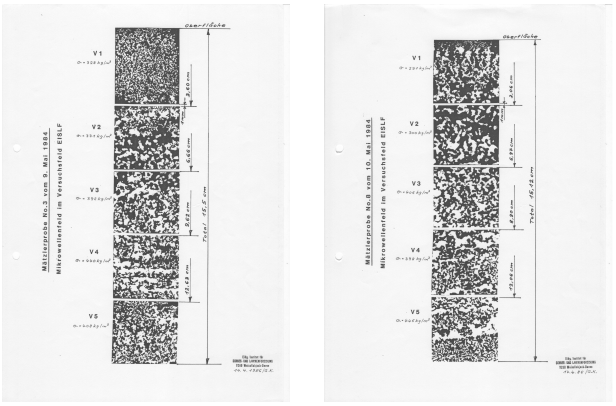

(a) (b)

Fig. 3. Thin section images from PAMIR melt-refreeze experiment. (a) May 9, 1984. (b) May 10, 1984.

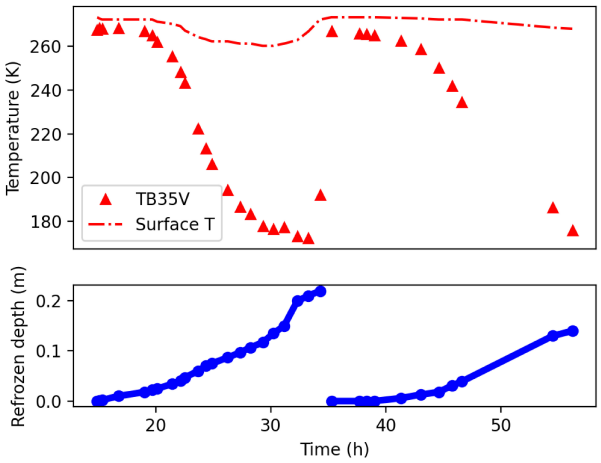

Fig. 4. Time series of refrozen snow depth (blue), surface temperature (red dot-dashed line) and observed brightness temperature at 35 GHz, vertical polarization (red triangles) for the PAMIR snow crust experiment, May 8–10, 1984.

Correlation functions were calculated in the z- and x-direction for each of the five subsections in both images and together with the layer thickness and density observations noted in the images were used to construct a time series of snowpacks of depth given by the refrozen thickness measurements shown in Fig. 4. Also shown in Fig. 4 is the decrease in surface temperature and snowpack brightness temperature at 35 GHz as the snowpack refreezes, with a sudden reversal as the snowpack, returns to a melting state. Table I gives a summary of the analytical microstructure model parameters derived from the thin section images, averaged over horizontal and vertical directions, where the y-direction parameters are assumed to be the same as in the x-direction.

These microstructural parameters were used to construct numerical snowpacks of time-dependent depth and assumed lower boundary emissivity of 96% at 0 °C. Sky T_B observations were used to parameterize a simple isotropic atmosphere, which was included in the simulations. The temperatures of the snow layer midpoints were calculated by linear interpolation between the melt interface at 0 °C and the observed

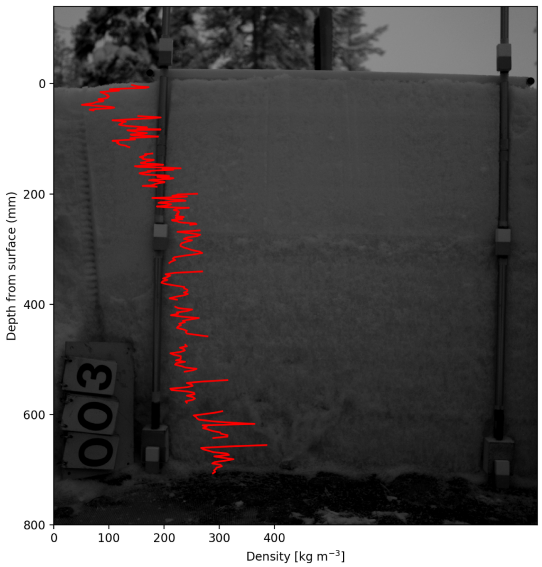

Fig. 5. NoSREx density derived from micro-CT samples overlaid on image of snowpit face. Sample taken on Mar. 1, 2012.

temperature at the snow surface. These data were used to drive SMRT simulations and were compared to the time series of passive data from the snow crust experiment (active data were not available for comparison).

C. Nordic Snow Radar Experiment (NoSREx)

The NoSREx took place in Sodankylä, Finland over four winter seasons and is described fully in [21]. The simulations presented here focus on the third season (2011–2012) where a near-complete micro-CT profile was available. Angular observations (30°–60°) of both T_B and backscatter (σ_0) are available for this campaign, and thus provides the first test of SMRT in active mode. An array of radiometers (V and H 10.65, 18.7, 21, 36.5 GHz) was installed on a tower 4.1 m above ground and a four-polarization scatterometer operating between 9.2 and 17.9 GHz was mounted 9.6 m above ground nearby. As with ASMEx, brightness temperature measurement error for 18.7–36.5 GHz radiometers is 1 K. Measurement error at 10.65 GHz is 2 K due to the radiometer design [21]. Backscatter measurement error is of the order 1 dB [21].

Fig. 5 illustrates the non-continuous density profile determined from micro-CT data. For simulation of a continuous snowpack, layers were constructed from each available micro-CT subsample and constant layer thickness derived from the automated sensor snow depth. The temperature profile of the snowpack was estimated by linear interpolation between automated measurements of the air temperature and 2 cm below the soil surface (mean of observations at two locations) limited to a maximum of 0°C. A summary of the microstructural parameters over this profile is given in Table I.

For the passive simulations, soil reflectivity was calculated with [32], assuming a soil roughness root mean square height of 2 cm. The soil permittivity was determined from the mean of two soil moisture measurements at 2 cm depth, soil sand content of 70%, clay content of 1% and dry density

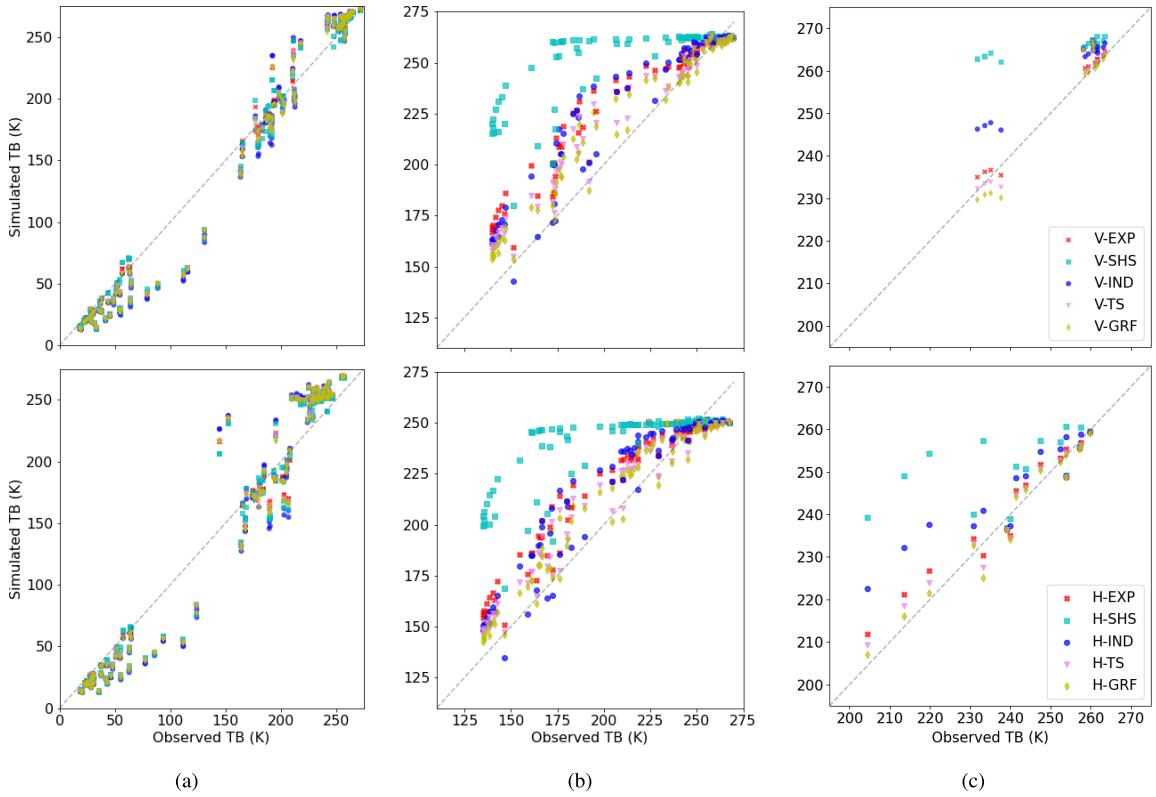

Fig. 6. Scatterplot comparison between observed and simulated brightness temperature (all frequencies observed, all incidence angles. V-polarization shown on top graphs, H-polarization shown on bottom. (a) ASMEx. (b) PAMIR. (c) NoSREx.

of 1300 $\mathrm{kg\,m^{-3}}$ with the model of [33]. The atmospheric contribution was approximated with nadir observations applied to the SMRT simple isotropic atmosphere, which will result in a small underestimation in T_B as a function of incidence angle. Rather than overfitting the soil contribution in the absence of data, a soil backscatter of -13 dB was assumed to be a reasonable approximation for both HH and VV polarization. For active simulations, micro-CT subsample layers were aggregated in groups of 20 so that the snowpack of 76 cm depth was represented by 16 layers for frequencies of 10.2, 13.3, and 16.7 GHz.

D. Microstructure Parameter Fitting

Similar to all datasets, the parameters for the SMRT microstructure models were obtained by fitting the autocorrelation functions obtained from binary 3-D micro-CT images (NoSREx, ASMEx) or 2-D binary thin sections images [PAMIR, cf. Fig. 3(a)]. All fits were done by using MATLAB's `lsqnonlin` optimization over a fixed number of data points (100) and allowing for a global normalization prefactor. The ice volume fraction (density) was obtained directly by counting the ice voxels/pixels of the images. The real space models (EXP, IND, TS, GRF) were fit along the main coordinate directions (x, y, z) of the 3-D/2-D correlation function yielding direction-dependent parameters that were subsequently averaged (arithmetic mean over directions) to obtain a single set of parameters for an isotropic model. For the isotropic Fourier model (SHS) the 3-D FT of the correlation function was spherically averaged and subsequently fit.

IV. SMRT Evaluation Results

A. Brightness Temperature

Brightness Temperature (T_B) observations were available for all field campaigns. Fig. 6 shows scatterplot comparisons between observed and simulated brightness temperature for each snow microstructural model and for each field campaign over all available frequencies. The ASMEx campaign observations in Fig. 6(a) cover a wider T_B range than PAMIR and NoSREx data due to the bottom boundary condition and shallow depth of snow: low T_B observations are of slabs on top of the metal plate and high T_B were observed after the plate had been removed and the snow was on top of the microwave absorbing material. The range of T_B measured in the PAMIR and NoSREx campaigns is smaller but is more representative of observations over natural snowpacks. The microstructure model appears to have only a small influence on the simulated T_B of the ASMEx slabs. Low T_B tends to be underestimated and high T_B overestimated for ASMEx. Outliers in the central range of observed values (approximately 100–150 K) were slabs A02, A04, and B07 at either 21 or 36.5 GHz. T_B at other frequencies for these slabs are more closely grouped with T_B of other slabs.

PAMIR data in Fig. 6(b) show a wide range of simulated T_B for a given observation e.g., an observed H-pol T_B of 175 K is represented by simulations over a range of 170–250 K.

TABLE II
BRIGHTNESS TEMPERATURE ME AND ROOT MEAN SQUARE ERROR (RMSE) [K]. SMALLEST ERRORS FOR EACH POLARIZATION ARE SHOWN IN BOLD FOR EACH FIELD EXPERIMENT

			EXP	SHS	IND	TS	GRF
ME	ASMEx	H	0.5	**0.2**	-0.3	-0.2	-0.3
		V	**-3.0**	-3.2	-4.0	-3.7	-3.9
	PAMIR	H	6.5	18.8	5.5	3.3	**2.1**
		V	7.3	18.9	6.2	4.0	**2.8**
	NoSREx	H	1.3	10.6	5.3	**0.2**	-0.6
		V	2.2	11.3	6.2	1.2	**0.3**
RMSE	ASMEx	H	22.7	**22.2**	25.1	23.3	23.2
		V	15.3	**15.0**	17.5	15.5	15.4
	PAMIR	H	15.2	35.1	14.5	11.6	**10.4**
		V	16.6	37.0	15.3	11.9	**10.2**
	NoSREx	H	4.3	17.1	9.0	3.6	**3.4**
		V	3.2	15.1	7.3	**3.1**	3.6

Simulated T_B are generally overestimated except at high T_B. However, the SHS microstructure model generally overestimates T_B by the largest amount. This is also the case for the NoSREx data in Fig. 6(c).

Given the more complicated structure of the full NoSREx snowpack, Fig. 6(c) highlights the overall importance of the microstructure model, particularly at lower T_B. For the NoSREx dataset, in general, the SHS model gives the highest T_B, followed by IND, EXP, TS, and with GRF giving the lowest T_B. A high SHS followed by EXP, TS, GRF in decreasing T_B order is also apparent in the PAMIR dataset, although IND can be above or below EXP, or have the lowest T_B of all microstructure models. In contrast, there is no consistency between the relative T_B given by different microstructure models in the ASMEx dataset: the order changes even for different micro-CT samples of the same slab.

Table II shows the mean error (ME) and root mean squared error (RMSE) for T_B simulated for each experiment. ME range from −4.0 to 0.5 K for ASMEx, 2.1 to 18.9 K for PAMIR and −0.6 to 11.3 K for NoSREx. RMSE ranges from 15.0–25.1 K for ASMEx, 10.2–37.0 K for PAMIR and 3.1–17.1 K for NoSREx. For the ASMEx field campaign, RMSE is the smallest for the SHS, with the smallest ME for SHS (H-pol), TS (H-pol), and EXP (V-pol) microstructures. In contrast, SHS performs poorly for both PAMIR and NoSREx experiments, with the largest ME and RMSE. For PAMIR and NoSREx experiments, TS and GRF microstructure models have the lowest ME and RMSE at both polarizations. The following subsections evaluate each field experiment, in turn, to explore these results further.

B. Scattering and Absorption Coefficients (ASMEx)

ASMEx data allow evaluation of SMRT absorption and scattering coefficients against those derived in [27], as shown in Figs. 7 and 8. A complete dataset is only available at 21 GHz due to instrumentation failure/installation dates at other frequencies. Calculation of the absorption coefficient (κ_a) in SMRT IBA is independent of microstructure model so Fig. 7 compares simulated κ_a (mean of subsamples) with observed κ_a for a single microstructure model. Note that κ_a in Fig. 7 have been scaled by 1/wavenumber to eliminate the direct

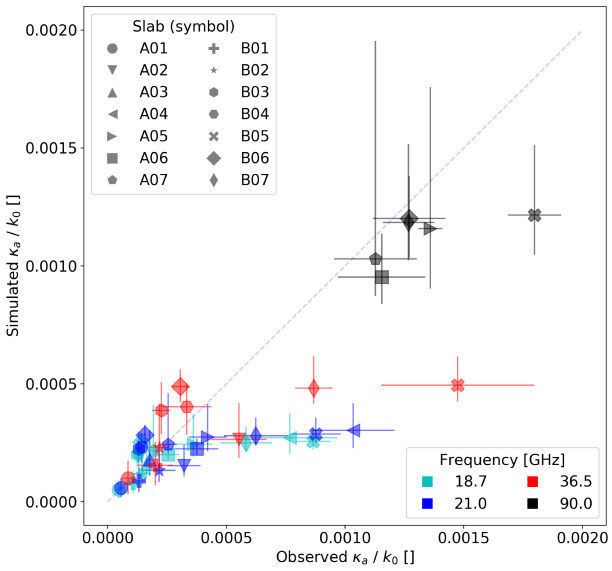

Fig. 7. Scatterplot of ASMEx subsample absorption coefficient, compared with observed absorption coefficient derived from observations in [27]. Coefficients have been normalized with respect to the wavenumber in free space, k_0. Note that the absorption coefficient is independent of the microstructure model. Observation error bars illustrate the difference between retrievals derived from H- and V-pol observations. Simulation error bars show the range of subsample absorption coefficients relative to the mean.

frequency dependence (an indirect dependence through the permittivity remains). In general, there is a good overlap with the 1:1 line, with a few noticeable outliers: slabs A02, A04, B05, and B07. Slab B05 (shown by crosses) was observed at all frequencies and its κ_a was consistently underestimated in the simulations. At 36.5 GHz, κ_a for slabs A02 (downward triangle) and B07 (thin diamond) were also underestimated, although slab B07 was simulated well at 90 GHz (A02 was not measured at this frequency). At 18.7 and 21 GHz, κ_a for slabs A04 (leftward triangle) and B07 were also underestimated. Comparing κ_a with observations for all slabs, the regression coefficient $r^2 = 0.94$, with RMSE of 0.3 m^{-1} and ME of −0.2 m^{-1}.

Unlike κ_a, scattering coefficients (κ_s) depend on microstructure model, as shown in Fig. 8. Note that κ_s has been shown on logarithmic axes. The comparison between models shows that for the ASMEx parameters, EXP, GRF, and TS models give near-identical results and there is also a high agreement between these models and IND. Lower regression coefficients were found between SHS and any other microstructure model, which reflect the increased scatter in SHS κ_s. For comparison with observations, the mean of subsample κ_s was compared with κ_s observed for the entire slab. Across all slabs, κ_s is generally overestimated at 90 GHz but underestimated at 36.5 GHz and below, with larger errors for lower scattering coefficients. This is not unexpected as observation errors and deficiencies in retrieval technique will have the greatest impact where the least scattering occurs. It is, however, difficult to apportion the discrepancies either to the frequency-dependence of IBA or to retrieval errors. Despite these differences, observations and simulations are highly correlated. Lowest r^2 between observed and simulated κ_s

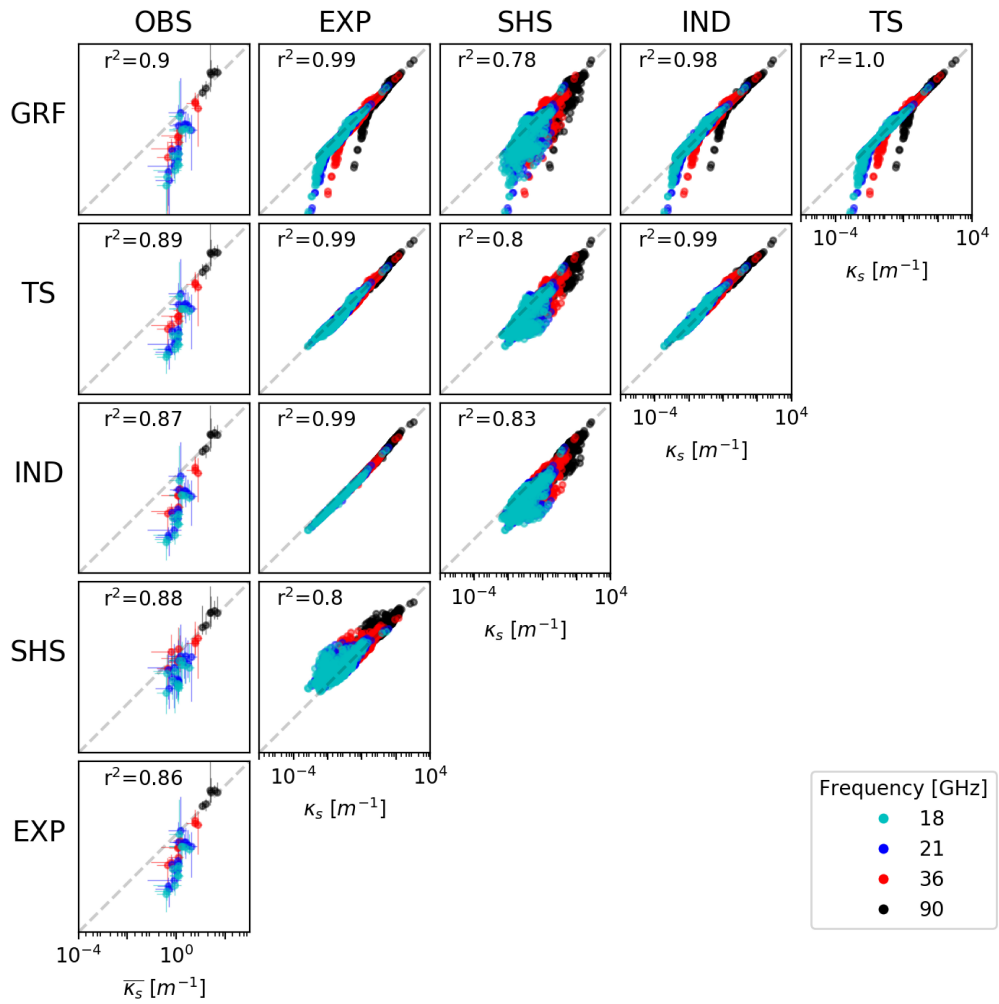

Fig. 8. Scatterplot comparison between scattering coefficients of different microstructure models from ASMEx subsamples, and a comparison of mean slab scattering coefficients with observed scattering coefficients from [27]. Gray dashed 1:1 line shown. As for Fig. 7, observation error bars illustrate the difference between retrievals derived from H- and V-pol observations. Simulation error bars show the range of subsample absorption coefficients relative to the mean.

occurred for the single length scale models EXP (0.86) and IND (0.87), median r^2 for SHS (0.88), and highest r^2 for the TS (0.89) and GRF (0.9) models. The difference between microstructure model correlation with observations suggests a choice of microstructure model influences the frequency dependence of IBA.

Errors in ASMEx T_B can be explained by κ_s at high T_B and κ_a at low T_B. At frequencies of 36.5 GHz and below, scattering coefficients are generally underestimated when compared with the retrieved values, which can explain overestimation of T_B at high T_B for the ASMEx data as there is a less simulated scattering of the radiation emitted from the absorber. For low T_B, where the substrate was a metal plate, differences in κ_s cannot explain the general underestimation in T_B. Outliers at these low T_B are generally for slabs A02, A04, B05, and B07, where κ_a and therefore the emission from the snow itself was underestimated. These particular slabs also formed outliers in the central range of ASMEx T_B. It is worth noting that slab B05 was considerably thinner (5.4 cm thickness) than other slabs (∼15 cm), which may have impacted the accuracy of retrieved κ_a and κ_s for that slab. Less accurate retrievals of κ_a and κ_s can be expected where scattering is low and could partially explain the underestimation of low κ_s in Fig. 8.

Vertical structures within snow assumed to be spherically isotropic resulted in higher T_B errors than for horizontal structures. Whilst ASMEx slabs were nominally selected for homogeneity within layers, this was not necessarily the case. In addition, analysis of correlation functions in x-, y-, and z-directions showed that the slabs were anisotropic (Fig. 2). Most of the slabs had an anisotropy factor <1, meaning greater correlation lengths in the horizontal than in the vertical. Only slabs A04, B05, and B07 showed anisotropy factors generally >1 i.e., larger correlation lengths in the vertical direction more commonly associated with vertical features such as depth hoar chains. Scattering and absorption coefficients and brightness temperature for these slabs were less well simulated than for other slabs.

C. Simple Snowpack (PAMIR)

Whilst Fig. 6(b) gives an overall picture of T_B simulations for a shallow refrozen snowpack with simple lower boundary condition, Fig. 9 examines the evolution of T_B over time as

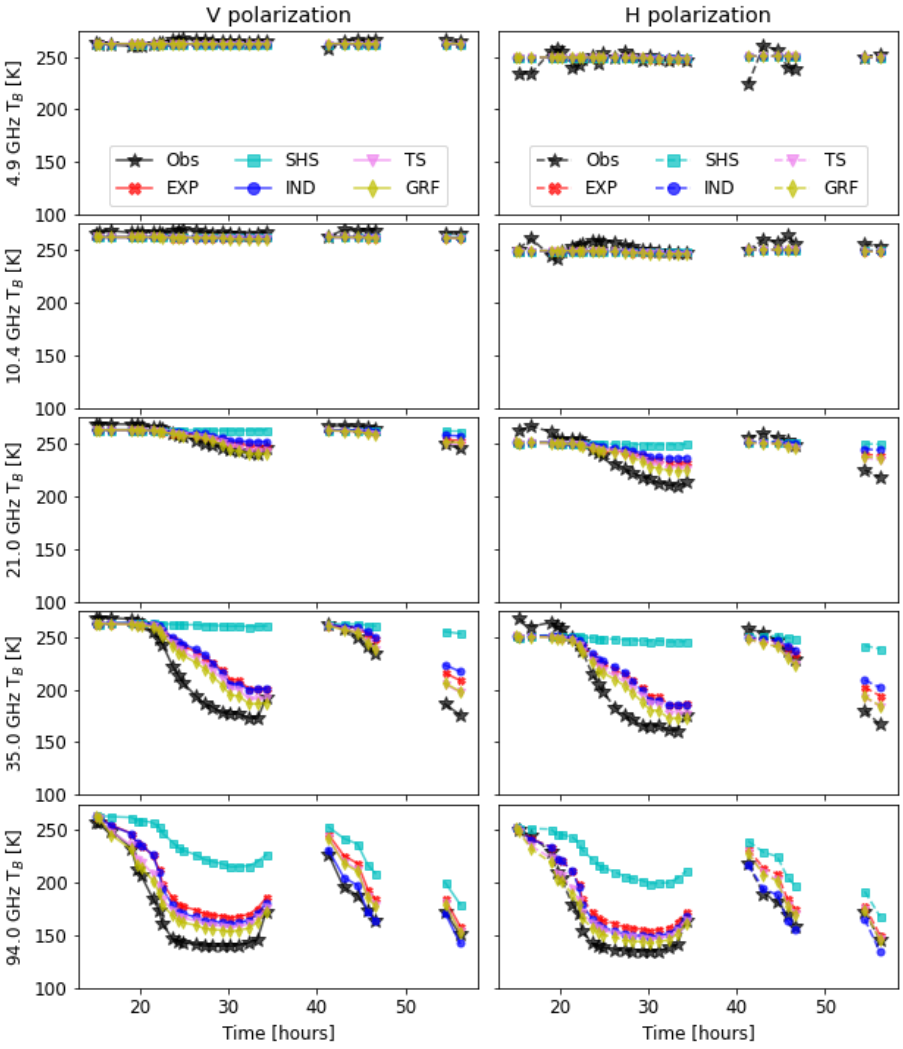

Fig. 9. Time series of brightness temperature for PAMIR experiment (periods with dry surface snow shown).

the snowpack refreezes. At 4.9 and 10.4 GHz, the impact of the snow–and therefore of the microstructure models–is small. There is more variability in the H-pol observations than at V-pol, but the simulations do not capture the observed variability in H-pol T_B. At higher frequencies, the contribution of the snow increases and the impact of the substrate diminishes. Simulations reflect the rapid decline in observed T_B with increasing depth of refrozen snow at 21 GHz and above although the observed rate at 35 GHz is faster than simulated. For much of the time series, the GRF model demonstrates the best agreement with observations. The SHS microstructure model does not show good agreement with observations at 21 and 35 GHz but is better able to capture the decline in T_B at 94 GHz for the second refreeze period. The difference in performance between models is shown in the ME in Table II, with TS and GRF demonstrating the lowest errors.

PAMIR is an ideal dataset for exploring reasons for different microstructure model performances as it is relatively small and there are large differences between microstructure models. Fig. 10 demonstrates how the correlation functions for different microstructure models, as used in SMRT after averaging, compare with observed correlation functions. Data for the 9th May have been shown as continuous T_B are available for this day. The dominant horizontal (crust) features evident in Sections 2–4 of Fig. 3(a) are reflected by the anisotropy in the real-space correlation function in Fig. 10, with high correlations in the x-direction tail. Section 5 has vertical features (high correlation in the z-direction tail) whereas Section I is relatively isotropic. The parameterized correlation functions thus always represent a compromise between the different coordinate directions.

For the real-space correlation functions it is possible to compare their performance via naive fit metrics (mean square error) which are shown in Table III. IND microstructure is the least-well fit microstructure parameter yet T_B errors in Table II are overall lower than for EXP. However, errors depend on frequency. At 21 GHz, Fig. 6(b) shows higher T_B errors with IND than EXP, but lower errors at 35 GHz and above. At small scales (e.g., $r \lesssim 1$ mm), the IND correlation function shown in Fig. 10 is higher than EXP and TS real-space microstructure models for Sections II–V, indicating more scattering. At larger scales, the lower IND correlation however would suggest less scattering than for other models. In Fourier space, smaller length scales (wavelengths) correspond to larger frequencies.

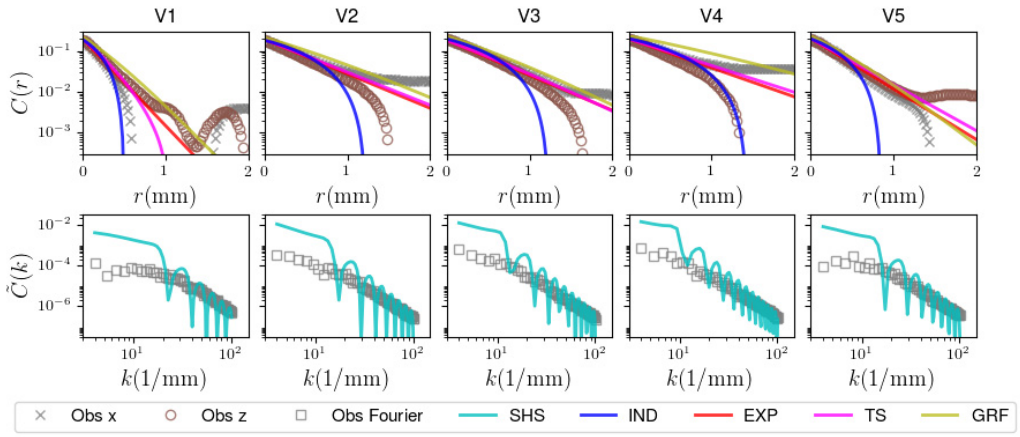

Fig. 10. Comparison between observed and parameterized correlation functions for EXP, IND, TS and GRF in real space (top) and SHS in Fourier space (bottom).

TABLE III
REAL-SPACE FIT METRICS IN x- AND z-DIRECTIONS FOR 9TH MAY PAMIR MICROSTRUCTURAL PARAMETERS, CALCULATED AS THE SUM OF THE SQUARED RESIDUALS OF THE NON-LINEAR FIT (*nonlinsq* MATLAB FUNCTION) OVER 100 DATA POINTS (MULTIPLIED BY 10^3). SHS IS EXCLUDED AS IT MUST BE FIT IN FOURIER SPACE AND IS NOT COMPARABLE

	IND		EXP		TS		GRF	
Layer	x	z	x	z	x	z	x	z
1 (top)	1.6	3.5	2.2	0.3	0.6	0.3	0.6	0.3
2	20.2	4.6	3.9	1.7	3.9	0.6	5.0	0.7
3	8.5	3.6	0.4	1.8	0.4	0.1	0.6	0.2
4	37.1	8.6	13.1	9.5	13.1	4.3	15.1	3.9
5	3.6	8.5	0.8	1.6	0.3	1.6	0.4	2.1

IND could have lower T_B errors than EXP at higher frequencies because of the poor but higher fit at small scales. IND correlation underestimation at larger scales is more relevant at lower frequencies and could explain why T_B is higher for IND than any other real-space microstructure model at low frequencies.

TS is a better fit to the measured correlation than EXP (although demonstrates EXP-behavior in the x-direction for Sections II–IV). The correlation is also higher than EXP at all scales. The larger TS scattering leads to lower T_B errors. GRF correlations are generally higher than TS, resulting in further reductions in T_B errors.

The interpretation of naive mean square fit errors must however be taken with caution: In real space the tail of the correlation function dominates the scattering coefficient while absolute values are very small, thus having a low influence on the fit error. This also prevents a direct comparison of fit metrics between real space models and Fourier models (like SHS). For SHS, Fig. 10 however visually reveals that the fit is poor, in particular for low k values. The difficulties of fitting the SHS sphere model to micro-CT data is well-known [14] and remains here the main reason for the poor performance of the SHS model. The comparison reveals that the details of the retrieval of microstructure parameters from CT or thin section image data are a critical, non-trivial problem that extends beyond the scope of this article. Implications and future work are indicated in the discussion.

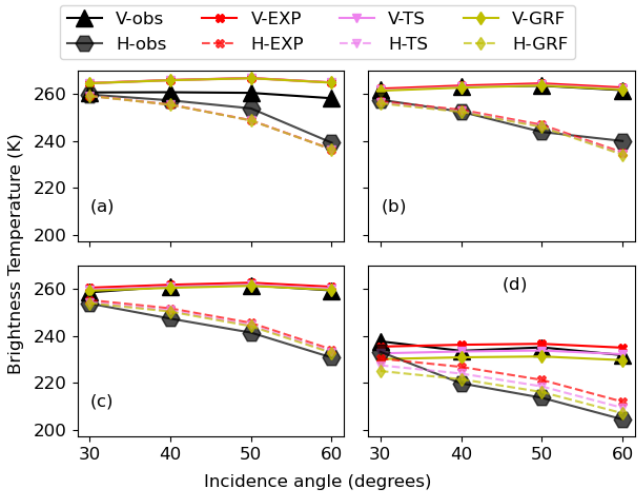

Fig. 11. Brightness temperature variation with incidence angle for NoSREx experiment on Mar. 1, 2012. (a) 10.65 GHz, (b) 18.7GHz, (c) 21 GHz, and (d) 36.5 GHz.

D. Complex Snowpack (NoSREx)

The NoSREx data provide an opportunity to evaluate SMRT for a deeper, more complex snowpack with soil substrate and a range of incidence angles. Fig. 11 shows the angular dependence of T_B for the EXP, TS and GRF models as these demonstrated the smallest errors in Table II. The difference between simulations for each microstructure model increased with increasing frequency. All three microstructure models agreed well with observations, with RMSE between 3.1 and 4.3 K, and all simulations generally followed the observed shape of the brightness temperature curves. At 21 and 36.5 GHz, T_B at H-pol were overestimated at incidence angles of 40° and larger.

The polarization difference at 10.65 GHz is too large for all microstructural models, which is an indication that the layer thicknesses could be too thin [34]. Layer thicknesses of 2.37 mm were taken directly from the resolution of the micro-CT data, but are actually smaller than the wavelength (28 mm). Resampling of the stratigraphic EXP microstructural properties from 320 to 16 layers of thickness 47.45 mm is

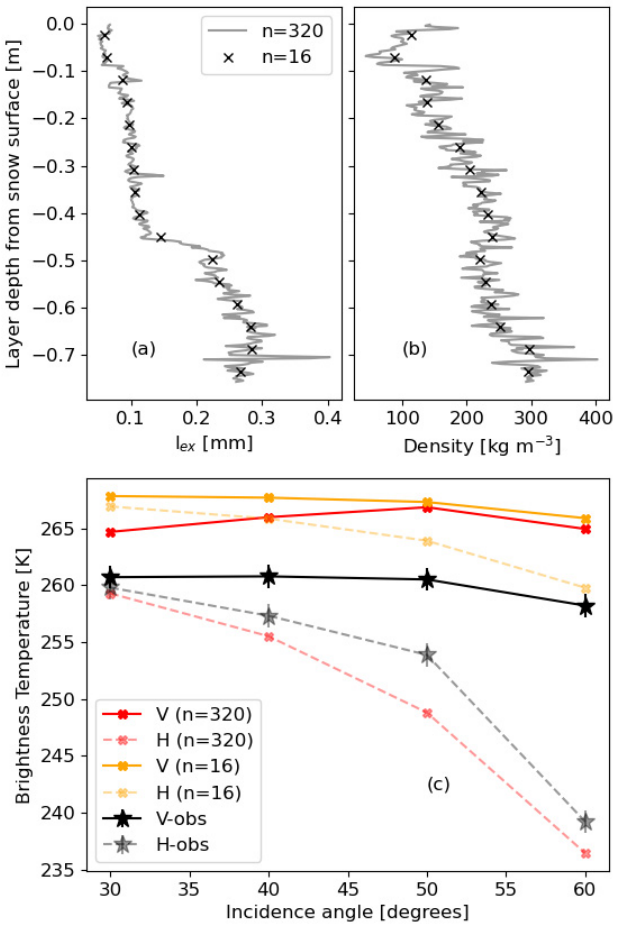

Fig. 12. Impact of changing stratigraphic resolution of (a) exponential correlation length and (b) density on (c) 10.65 GHz T_B curves. High resolution (HR) simulations have 320 layers whereas low resolution (LR) have 16 layers.

illustrated in Fig. 12(a) and (b). Resampling captured the trend in density and exponential correlation length, but not the high densities and exponential correlation lengths observed in some thin layers at the base of the snowpack. The effect of lower resolution stratigraphy on simulated T_B at 10.65 GHz is shown in Fig. 12(c). Both H- and V-pol T_B increased, with a greater impact at H-pol. This narrowed the polarization difference, but at the cost of T_B simulation accuracy.

E. Backscatter

Simulations of total backscatter (σ_0) with the lower resolution NoSREx snowpack are shown in Fig. 13. No observations were made of the bare soil backscatter (σ_s), so the relative accuracy of the simulations is linked to the chosen parameterization of $\sigma_s = -13$ dB. Consequently, no error metrics have been presented and it is not possible to conclude any one microstructure model is a better representation than any other. These simulations are intended to highlight differences (or lack of differences) between microstructure models over a range of incidence angles.

As with the passive simulations, microstructure model differences shown in Fig. 13 are greater at higher frequencies. σ_0 was highest for the TS model (closely followed by GRF), and lowest for the SHS microstructure model. At 16.7 GHz

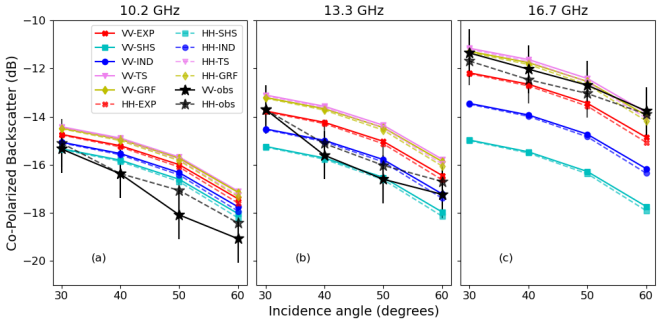

Fig. 13. Comparison between SMRT simulated backscatter and NoSREx observations on Mar. 1, 2012. Panels (a)–(c) show copolarized backscatter, whereas panels (d)–(f) show cross-polarized backscatter. 1 dB measurement error shown.

and incidence angle of 50°, σ_0 for TS microstructure was −12.4 dB, but −16.3 dB for SHS microstructure. Differences between VV and HH σ_0 were smaller in the simulations than observations, with a larger decrease in HH σ_0 with incidence angle than for VV. At 10.2 and 13.3 GHz observed HH σ_0 was higher than VV σ_0, whereas at 16.7 GHz, VV σ_0 is higher than HH σ_0. For all simulations, VV σ_0 is higher than HH σ_0. Cross-polarization simulations have not been presented as SMRT does not currently account for cross-polarization backscatter contribution from the substrate.

Copolarized backscatter behavior is broadly captured by SMRT, but the difference between microstructure models can exceed measurement error. No conclusions can be drawn as to the most appropriate microstructure for these data due to uncertainty in the soil backscatter contribution. Improved knowledge of substrate reflectivity is key to demonstrating simulation accuracy.

V. Discussion

SMRT accuracy in this study is comparable to or better than other studies, but the main improvement is that it is achieved without *ad hoc* scaling or optimization of microstructure parameters. The snow parameters are purely based on *in situ* measurements. Evaluation of SMRT against these data shows the largest RMSE for the ASMEx dataset and the smallest for NoSREx. ASMEx RMSE errors are similar to those found in [18], where mean RMSE in the frequency range 19–89 GHz for both Arctic and Sub-Arctic snow was 16 and 23 K for EXP and SHS microstructure, respectively. While RMSE is comparable for ASMEx, the ME is lower than in [18]. Studies with other microwave emission models indicate mean RMSE (19–37 GHz) of around 13 K [10] and 16–26 K [12], but as with [18], these were based on microstructure optimization techniques not applied here. Improvements in SMRT simulations come from the ability to determine and use microstructural parameters directly from micro-CT or thin section images, and from new microstructural models available in SMRT.

Precisely how microstructure parameters are derived requires further attention in a number of areas: 1) fit technique, 2) anisotropy, and 3) stratigraphy. The current method used to fit the analytical microstructure models to the measured correlation function places no weight on different portions of

the curve, meaning fits can be worse at length scales more relevant to particular frequencies.

SHS cannot easily be compared with other microstructure models because the fit to micro-CT data must be done in Fourier space. SHS did not perform well for PAMIR and NoSREx, yet has the potential to perform well as shown by ASMEx. It is difficult to retrieve parameters for the SHS model [14] as the retrieval tends to identify the lowest possible stickiness as shown in Table I. The fit of the SHS correlation function to experimental data is subject to degeneracy: similar goodness of fits can be obtained by simultaneous variation of diameter and stickiness. For PAMIR, fits to the correlation function at low k are relatively poor and these parameters are likely more representative at higher frequencies. Microstructure models that have both real-space and Fourier-space analytical correlation functions (IND, EXP, TS) could be used to provide insight into fitting methodology e.g., whether better results can be obtained by fitting in Fourier space. This would also allow us to assess whether it is advantageous to perform the orientational averaging of anisotropic snow in real or Fourier space.

Anisotropy has been demonstrated here, even in snow that visually appears homogeneous, and snow with predominantly vertical structures is simulated less well. The simple assumption applied here was that the isotropic parameters currently required in SMRT could be represented by an equally weighted average of microstructure parameters derived along Cartesian directions. As scattering is non-linearly related to microstructure parameters, this may not be the best approach. Non-equal weight given to the microstructural length scales observed in multiple directions could be explored in the first instance and fitting to the directionally averaged correlation function could also be tested, although a fundamental advancement in SMRT may be needed to account for anisotropic media properly.

There are greater differences between microstructure models for PAMIR than for ASMEx, despite similar snow depths and substrate (absorber). This could be a function of greater snow heterogeneity in the PAMIR experiment than for ASMEx, but more likely because of generally coarser structures (Table I) enhancing the sensitivity to microstructure. PAMIR provides interesting data. In this study, ice lenses were not treated as separate thin layers, so there is potential to improve simulations further through explicit consideration of coherence and interlayer boundary effects. However, the better performance of TS and GRF compared with other microstructure models within SMRT may mean that the secondary structure parameter is partially able to compensate for coherent and semicoherent effects.

More generally, we need to rethink how we consider snowpack layers. Snow layers for simulations are often defined by the resolution of the field measurements. Micro-CT allows very fine resolution information, potentially at a higher resolution than microwave observations are sensitive to. At 37 GHz the wavelength is 8 mm whereas at 10 GHz it is 30 mm. Since the RT theory is based on energy transport without tracking the wave phase, specification of thinner layers than the wavelength introduces artificial dielectric discontinuities, which leads to overestimated polarization difference in the simulations [34]. SMRT is equipped with a correction for a subwavelength thin layer surrounded by two normal layers, which is relevant for modeling ice lenses, but as with any RT model, SMRT is not able to deal with a snowpack with many layers thinner than the wavelength properly.

PAMIR microstructural parameters were derived from $\sim$5 cm sections, which are much larger than the wavelengths of the observations. ASMEx layers range from 6 mm to 9 mm in thickness: still too fine for the simulations given that the longest wavelength considered is 16 mm. For homogeneous slabs, this would not matter, but vertical bars for simulated κ_s in Fig. 8 indicate a fair degree of variability in many of the slabs. Agreement with retrieved κ_s depends on whether the slabs conform with the retrieval assumptions, but even good simulations of κ_s can lead to poor T_B simulations if there are more dielectric discontinuities simulated than observed by the sensors. This does not appear to be a problem for the ASMEx dataset but is for NoSREx at 10 GHz where the layers are thinner and a longer wavelength considered. This only concerns H-pol simulations, particularly at large incidence angles.

Larger micro-CT sampling size allows longer tail correlation function analysis but it is not clear whether layers could then become too large in the simulation and neglect dielectric discontinuities observed by the sensor (e.g., single layer snowpack simulations are generally insufficient) so the question is what is the most appropriate resolution for snowpack stratigraphy? Micro-CT should be used to address this question with the added benefit of informing resolution of future field campaigns to minimize micro-CT processing cost.

Some of the above questions could be addressed by using the measured correlation functions directly in SMRT. This is theoretically possible but needs more understanding of how to prevent numerical instabilities caused by the tail of non-decaying correlation functions. Nevertheless, micro-CT offers the potential to look at microstructure in a way that has not been possible previously and offers a pathway to more accurate simulations. However, field sampling is not as easy as for other microstructural observation methods (e.g., SSA and density), and the laboratory processing to extract the 3-D structure is expensive. More work is needed to speed up the micro-CT processing chain and/or develop strategies for relating field measurable quantities to the microstructural model parameters needed for more accurate simulations.

Accurate quantification of simulation errors is critical for remote sensing applications. For some applications, snow may not be the primary focus but affects the measurements so it is necessary to understand the contribution of snow to the observation error budget in e.g., ice thickness retrievals. In numerical weather prediction, atmospheric observation uncertainty due to snow is an essential requirement for the assimilation of microwave data in lower troposphere sounding channels. SMRT can also be used in the design of future snow monitoring missions for water supply management.

VI. Conclusion

This article evaluated SMRT against three field experiments of differing snowpack complexity and covers a range in

snow type, snow depth, and observation incidence angle. The way snow microstructure is quantified can have a dramatic impact on the simulation of microwave brightness temperature or backscatter and becomes increasingly important at higher frequencies. The optimum microstructure model may depend on snow type, and the new two-parameter TS and GRF microstructure models give more accurate brightness temperature simulations than other microstructure models for two of the three field campaigns evaluated.

At present, micro-CT or thin section images are needed to determine the necessary microstructure parameters. Future research should focus on the following: 1) assess methods to fit microstructure models to micro-CT data 2) how to parameterize microstructure models from field observations, 3) how to treat snowpack layers given that different frequencies observe different dielectric discontinuities, 4) how to account for anisotropy in the microstructure, and (v) quantifying simulation uncertainties in support of remote sensing applications. SMRT provides the framework to do this.

VII. Code Availability

Code and data to run these simulations are available from https://github.com/smrt-model/smrt_evaluation_paper

Acknowledgment

The authors would like to thank all contributors to SMRT development and testing. Staff at Finnish Meteorological Institute are acknowledged for assisting in data collection for the NoSREx and ASMEx campaigns. The authors would also like to thank the Reviewers for their careful consideration and comments that have helped improve this article, particularly the suggestion to include microstructure fit metrics.

References

[1] G. Picard, M. Sandells, and H. Löwe, "SMRT: An active–passive microwave radiative transfer model for snow with multiple microstructure and scattering formulations (v1.0)," *Geosci. Model Develop.*, vol. 11, no. 7, pp. 2763–2788, Jul. 2018. [Online]. Available: https://www.geosci-model-dev.net/11/2763/2018/

[2] A. Kontu and J. Pulliainen, "Simulation of spaceborne microwave radiometer measurements of snow cover using *in situ* data and brightness temperature modeling," *IEEE Trans. Geosci. Remote Sens.*, vol. 48, no. 3, pp. 1031–1044, Mar. 2010.

[3] J. T. Pulliainen, J. Grandell, and M. T. Hallikainen, "HUT snow emission model and its applicability to snow water equivalent retrieval," *IEEE Trans. Geosci. Remote Sens.*, vol. 37, no. 3, pp. 1378–1390, May 1999.

[4] J. Lemmetyinen, J. Pulliainen, A. Rees, A. Kontu, Y. Qiu, and C. Derksen, "Multiple-layer adaptation of HUT snow emission model: Comparison with experimental data," *IEEE Trans. Geosci. Remote Sens.*, vol. 48, no. 7, pp. 2781–2794, Jul. 2010.

[5] C. Mätzler, "Relation between grain-size and correlation length of snow," *J. Glaciol.*, vol. 48, no. 162, pp. 461–466, 2002.

[6] A. Wiesmann and C. Mätzler, "Microwave emission model of layered snowpacks," *Remote Sens. Environ.*, vol. 70, no. 3, pp. 307–316, Dec. 1999. [Online]. Available: https://www.sciencedirect.com/science/article/pii/S0034425799000462

[7] C. Mätzler and A. Wiesmann, "Extension of the microwave emission model of layered snowpacks to coarse-grained snow," *Remote Sens. Environ.*, vol. 70, no. 3, pp. 317–325, Dec. 1999. [Online]. Available: https://www.sciencedirect.com/science/article/pii/S0034425799000474

[8] L. Brucker *et al.*, "Modeling time series of microwave brightness temperature at dome C, Antarctica, using vertically resolved snow temperature and microstructure measurements," *J. Glaciol.*, vol. 57, no. 201, pp. 171–182, 2011.

[9] G. Picard *et al.*, "Simulation of the microwave emission of multilayered snowpacks using the dense media radiative transfer theory: The DMRT-ML model," *Geosci. Model Develop.*, vol. 6, no. 4, pp. 1061–1078, Jul. 2013. [Online]. Available: https://www.geosci-model-dev.net/6/1061/2013/

[10] A. Roy *et al.*, "Brightness temperature simulations of the Canadian seasonal snowpack driven by measurements of the snow specific surface area," *IEEE Trans. Geosci. Remote Sens.*, vol. 51, no. 9, pp. 4692–4704, Sep. 2013.

[11] N. Rutter *et al.*, "Snow stratigraphic heterogeneity within ground-based passive microwave radiometer footprints: Implications for emission modeling," *J. Geophys. Research: Earth Surf.*, vol. 119, no. 3, pp. 550–565, Mar. 2014, doi: 10.1002/2013JF003017/abstract.

[12] A. Royer *et al.*, "Comparison of commonly-used microwave radiative transfer models for snow remote sensing," *Remote Sens. Environ.*, vol. 190, pp. 247–259, Mar. 2017. [Online]. Available: https://www.sciencedirect.com/science/article/pii/S0034425716304990

[13] M. Sandells, R. Essery, N. Rutter, L. Wake, L. Leppänen, and J. Lemmetyinen, "Microstructure representation of snow in coupled snowpack and microwave emission models," *Cryosphere*, vol. 11, no. 1, pp. 229–246, Jan. 2017. [Online]. Available: https://www.the-cryosphere.net/11/229/2017/

[14] H. Löwe and G. Picard, "Microwave scattering coefficient of snow in MEMLS and DMRT-ML revisited: The relevance of sticky hard spheres and tomography-based estimates of stickiness," *Cryosphere*, vol. 9, no. 6, pp. 2101–2117, Nov. 2015.

[15] M. Durand, E. J. Kim, and S. A. Margulis, "Quantifying uncertainty in modeling snow microwave radiance for a mountain snowpack at the point-scale, including stratigraphic effects," *IEEE Trans. Geosci. Remote Sens.*, vol. 46, no. 6, pp. 1753–1767, Jun. 2008.

[16] B. Montpetit *et al.*, "New shortwave infrared albedo measurements for snow specific surface area retrieval," *J. Glaciol.*, vol. 58, no. 211, pp. 941–952, 2012.

[17] M. Kerbrat, B. Pinzer, T. Huthwelker, H. W. Gäggeler, M. Ammann, and M. Schneebeli, "Measuring the specific surface area of snow with X-ray tomography and gas adsorption: Comparison and implications for surface smoothness," *Atmos. Chem. Phys.*, vol. 8, no. 5, pp. 1261–1275, Mar. 2008. [Online]. Available: https://hal.archives-ouvertes.fr/hal-00296473

[18] C. Vargel *et al.*, "Arctic and subarctic snow microstructure analysis for microwave brightness temperature simulations," *Remote Sens. Environ.*, vol. 242, Jun. 2020, Art. no. 111754. [Online]. Available: https://www.sciencedirect.com/science/article/pii/S0034425720301243

[19] W. Maslanka *et al.*, "Arctic snow microstructure experiment for the development of snow emission modelling," *Geosci. Instrum., Methods Data Syst.*, vol. 5, no. 1, pp. 85–94, Apr. 2016. [Online]. Available: https://www.geosci-instrum-method-data-syst.net/5/85/2016/

[20] B. Reber, C. Mätzler, and E. Schanda, "Microwave signatures of snow crusts modelling and measurements," *Int. J. Remote Sens.*, vol. 8, no. 11, pp. 1649–1665, Nov. 1987, doi: 10.1080/01431168708954805.

[21] J. Lemmetyinen *et al.*, "Nordic snow radar experiment," *Geosci. Instrum., Methods Data Syst. Discuss.*, vol. 5, no. 2, pp. 1–23, 2016. [Online]. Available: https://www.geosci-instrum-method-data-syst-discuss.net/gi-2015-29/

[22] C. Mätzler, "Improved born approximation for scattering of radiation in a granular medium," *J. Appl. Phys.*, vol. 83, no. 11, pp. 6111–6117, Jun. 1998, doi: 10.1063/1.367496.

[23] A. Sihvola, *Electromagnetic Mixing Formulas and Applications*. London, U.K.: Institution of Engineering and Technology, Jun. 1999.

[24] W. Dierking, S. Linow, and W. Rack, "Toward a robust retrieval of snow accumulation over the antarctic ice sheet using satellite radar," *J. Geophys. Res., Atmos.*, vol. 117, no. D9, pp. 1–17, May 2012, doi: 10.1029/2011JD017227.

[25] L. Tsang, J. Pan, D. Liang, Z. Li, D. W. Cline, and Y. Tan, "Modeling active microwave remote sensing of snow using dense media radiative transfer (DMRT) theory with multiple-scattering effects," *IEEE Trans. Geosci. Remote Sens.*, vol. 45, no. 4, pp. 990–1004, Apr. 2007.

[26] M. Teubner, "Level surfaces of Gaussian random fields and microemulsions," *Europhys. Lett.*, vol. 14, no. 5, pp. 403–408, Mar. 1991, doi: 10.1209/0295-5075/14/5/003.

[27] W. Maslanka *et al.*, "Derivation and evaluation of a new extinction coefficient for use with the n-HUT snow emission model," *IEEE Trans. Geosci. Remote Sens.*, vol. 57, no. 10, pp. 7406–7417, Oct. 2019.

[28] W. M. Maslanka, "Extinction of microwave radiation in snow," Ph.D. dissertation, Dept. Meteorol., Univ. Reading, Reading, U.K., 2017. [Online]. Available: https://centaur.reading.ac.uk/72703/

[29] S. Leinss, H. Löwe, M. Proksch, and A. Kontu, "Modeling the evolution of the structural anisotropy of snow," *Cryosphere*, vol. 14, no. 1, pp. 51–75, Jan. 2020. [Online]. Available: https://tc.copernicus.org/articles/14/51/2020/
[30] C. Mätzler and A. Wiesmann, "Documentation for MEMLS, version 3, microwave emission model of layered snowpacks," MEMLS Manual, Version: 03.07.14, 14:52, Tech. Rep., Jul. 2014, p. 26.
[31] C. Mätzler, "Applications of the interaction of microwaves with the natural snow cover," *Remote Sens. Rev.*, vol. 2, no. 2, pp. 259–387, Jan. 1987, doi: 10.1080/02757258709532086.
[32] U. Wegmüller and C. Mätzler, "Rough bare soil reflectivity model," *IEEE Trans. Geosci. Remote Sens.*, vol. 37, no. 3, pp. 1391–1395, May 1999.
[33] M. Dobson, F. Ulaby, M. Hallikainen, and M. El-rayes, "Microwave dielectric behavior of wet soil-part II: Dielectric mixing models," *IEEE Trans. Geosci. Remote Sens.*, vol. GE-23, no. 1, pp. 35–46, Jan. 1985.
[34] M. Leduc-Leballeur *et al.*, "Modeling L-band brightness temperature at dome C in Antarctica and comparison with SMOS observations," *IEEE Trans. Geosci. Remote Sens.*, vol. 53, no. 7, pp. 4022–4032, Jul. 2015.

Melody Sandells received the M.Sci. degree in physics from Imperial College London, London, U.K., in 1998, and the Ph.D. degree from the University of Reading, Reading, U.K., in 2002.

She held Postdoctoral Research Positions with the Center for Polar Observation and Modeling, University College London and within the National Center for Earth Observation, University of Reading. She later became the Director of CORES Science and Engineering Limited, U.K., and was appointed as a Senior Lecturer with the Department of Geography and Environmental Sciences, Northumbria University, Newcastle upon Tyne, U.K., in 2020. She is the President-Elect of the International Commission on Snow and Ice Hydrology. Her research interests include snow and cryosphere physics, earth observation of snow and soil moisture, and soil-snow-vegetation radiative transfer (RT) at optical, thermal, and microwave wavelengths.

Henning Löwe received the Diploma degree in physics and the Ph.D. degree in theoretical physics from the University of Göttingen, Göttingen, Germany, in 1999 and 2004, respectively.

His post-doctoral research focused on topics in atmospheric sciences and snow physics. Since 2011, he has been a Lecturer with the Department of Earth Sciences at ETH, Zurich and since 2018, he has been the Head of the Research Group Snow Physics, WSL Institute for Snow and Avalanche Research SLF, Davos, Switzerland. His work is dedicated to microstructure controls on mechanical, thermal, electromagnetic, and crystal growth processes in snow.

Ghislain Picard received the M.Sc. degree in remote sensing from the University of Paris VII, Paris, France, in 1997, and the Ph.D. degree from Center d'Etudes Spatiale de la Biosphere (CESBIO), Toulouse, France, in 2002.

During his Ph.D., he developed several electromagnetic models of vegetation backscatter in the microwave range. After postdoctorate research with the Centre for Terrestrial Carbon Dynamics, University of Sheffield, Sheffield, U.K., he joined the Laboratoire de Glaciologie et Géophysique de l'Environnement, Institut des Géosciences de l'Environnement, Université Grenoble Alpes, Grenoble, France, where he has been working since 2005. His main research is on the Antarctic climate observed through the study of snow using a variety of remote sensing techniques and field experimentation. He is involved in the development of innovative instruments for the characterization of the snow physical properties and of optical and microwave radiative transfer (RT) models.

Marie Dumont received the M.Sc. degree in remote sensing from the Université Paris 6, Paris, France, in 2007, and the Ph.D. degree from Paris East University, Paris, in 2010.

From 2007 to 2010, she conducted the Ph.D. work with the Institut des Geosciences de l'Environnement, Grenoble, France, where she developed several methods to retrieve snow and ice albedo from remote sensing data. After a Postdoctoral Research Position with Norwegian Polar Institute, Tromsø, Norway, in 2011, she joined the Center d'Etudes de la Neige (Center National de Recherches Météorologiques), Grenoble. Since then, her research has focused on the optical properties of snow, snow detailed modeling, and data assimilation.

Richard Essery received the B.Sc. degree in mathematical physics from the University of Edinburgh, Edinburgh, U.K., in 1987, the certificate of advanced studies in mathematics from the University of Cambridge, Cambridge, U.K., in 1988, and the Ph.D. degree in physics from the University of Cambridge in 1992.

He was a member of the Land Surface Processes Group, Met Office Hadley Center from 1992 to 2002, with responsibility for the representation of surface snow processes in global climate modeling. He took a sabbatical in 1998 with the Canadian National Hydrological Research Institute. In 2002, he joined the Center for Glaciology, University of Aberystwyth, Aberystwyth as the Natural Environment Research Council (NERC) Advanced Research Fellow, conducting field research in mountain hydrology and micrometeorology in Canada, United States, Sweden, and Switzerland. He has been with the School of Geosciences, University of Edinburgh, since 2007 and a Professor of cryosphere-atmosphere interactions since 2018. He is also the Secretary General of the International Association of Cryospheric Sciences.

Nicolas Floury received the M.Sc. degree in engineering from Télécom Paris Tech, Paris, France, in 1993, and the Ph.D. degree in applied physics from the University Paris Diderot, Paris, France, in 1999.

Since then, he has been with the European Space Research and Technology Center, European Space Agency, Noordwijk, The Netherlands, where he is the Head of the Wave Interaction and Propagation Section. His research interests include signal processing and electromagnetic modeling applied to microwave interaction with natural media.

Anna Kontu received the M.Sc.(Tech.) degree from the Helsinki University of Technology (part of Aalto University), Espoo, Finland, in 2006, and the D.Sc.(Tech.) degree from Aalto University, Espoo, Finland, in 2018.

She works as a Sodankylä Research Infrastructure Principal Investigator (PI) with the Finnish Meteorological Institute's Arctic Space Center, Sodankylä, Finland. Her research activities focus on microwave remote sensing of seasonal terrestrial snow and soil frost.

Juha Lemmetyinen received the D.Sc.(Tech.) degree in electrical engineering from Aalto University [former Helsinki University of Technology, TKK], Espoo, Finland, in 2012.

From 2004 to 2008, he was a Researcher with the TKK Laboratory of Space Technology, Department of Radio Science and Engineering, where he specialized in radiometer calibration techniques and remote sensing. From 2009 to 2013, was a Scientist with the Arctic Research Unit, Finnish Meteorological Institute, Helsinki, Finland. Since 2014, he has been acted as the Head of group at FMI for research on cryosphere processes. His present research interests include applications of microwave radiometers and synthetic aperture radar in remote sensing snow, soil and vegetation, including the development of emission and backscatter models.

William Maslanka received the M.Met. degree in meteorology and the Ph.D. degree in remote sensing and radiative modeling of snow from the University of Reading, Reading, U.K., in 2013 and 2017, respectively.

From 2017 to 2019, he was a Flood Modeler and a Forecaster with the Environment Agency, before returning to the University of Reading as a Researcher. His research interests include microwave remote sensing of surface soil moisture, the applications of drones to remote sensing techniques, and the remote sensing of snow.

Samuel Morin received the Ph.D. degree in environmental sciences in 2008.

In 2008, he worked on isotopic analyses of atmospheric nitrate in remote areas, he has worked since 2009 with the Snow Research Center (CEN, a research unit of the Center National de Recherches Météorologiques, CNRM, www.umr-cnrm.fr, affiliated to Météo-France and CNRS) where he coordinated several research initiatives relevant to the observation and modeling of the mountain snow cover, across various time and space scales. Most recently, he served as a Lead Author of the Intergovernmental Panel on Climate Change (IPCC) Special Report on Ocean and Cryosphere in a Changing Climate (SROCC) approved in September 2019. He is a Research Scientist with over ten years experience in the field of snow science.

Andreas Wiesmann (Senior Member, IEEE) received the Diploma degree in physics from the Institute of Applied Physics, University of Bern, Bern, Switzerland, in 1994, and the Ph.D. degree in natural sciences from the University of Bern in 1998.

Since 1998, he has been with GAMMA Remote Sensing AG, Gümligen, Switzerland. His research interests include the interaction of microwaves with natural targets, microwave hardware development, distributed high performance computing, large scale data processing, and computer security.

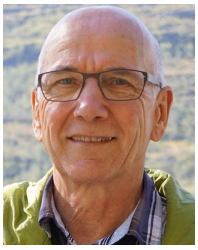

Christian Mätzler was born in Kreuzlingen, Switzerland, in 1945. He received the M.Sc. degree physics with minors in mathematics and geography from the University of Bern, Bern, Switzerland, in 1970, and the Ph.D. degree in solar radio astronomy from the University of Bern in 1974.

After postdoctoral research with the NASA Goddard Space Flight Center, Greenbelt, MD, USA, and Swiss Federal Institute of Technology (ETH), Zürich, Switzerland, he became a Research Group Leader for terrestrial and atmospheric radiometry and remote sensing with the Institute of Applied Physics, University of Bern, in 1978. There he received the habilitation in applied physics in 1986 and the title of a Titular Professor in 1992. He spent sabbaticals with the Universities of Colorado and Washington, in 1996, and at the Paris Observatory, in 2004. After retirement in July 2010, he started as a Consultant for Gamma Remote Sensing. His studies have concentrated on microwave (1–100 GHz) signatures for active and passive remote sensing of the atmosphere, snow, ice, soil, and vegetation, as well as on the development of methods for dielectric and propagation measurements for such media. He is an Editor of a book on thermal microwave emission with applications in remote sensing. He is interested in physical processes acting at the earth surface and in the atmosphere.